A Method to Trace Porphyromonas gingivalis Within Periodontal Ligament in 3D

A Method to Trace *Porphyromonas gingivalis* Within Periodontal Ligament in 3D

A Thesis Presented by
Andy Sungmin Lee

To
The Faculty of Harvard School of Dental Medicine
In partial fulfillment of the requirements for the degree of Doctorate of Medical Science (DMSc)

Research Mentor: Dr. Gili Naveh, Assistant Professor of Oral Medicine, Infection and Immunity

Harvard School of Dental Medicine

Boston, Massachusetts

April 2021

Abstract

Background and Objective: Periodontitis is an inflammatory disease caused by bacterial dysbiosis that leads to tooth support loss and eventually, loss of tooth. There have been studies using micro-CT, histology, and electron microscopy to elucidate the pathological effect of the pathogens in periodontal disease; however, the exact trace of these bacteria in inflamed periodontal tissue remains unclear. The purpose of this study was to develop a 3D imaging method that elucidates the distribution of *P. gingivalis* within periodontal ligament (PDL) upon infection, combining an optical clearing method, fluorescent-labeling via click chemistry, and multi-photon microscopy.

Materials and methods: Periodontal disease was induced by using 5-0 silk ligature in C57BL/6 mice. *P.g* was labeled with fluorophore via click chemistry, then introduced to the sulcus by tying 7-0 silk ligature. Optical clearing of dissected hemi-mandibles was achieved by ECi-based clearing method. Multi-photon microscopy was utilized to obtain 3D images of 2-photon signals from the fluorophore and SHG signals from type I collagen in PDL. Fluorescent bacteria in 2-photon images were detected by trained Zen Intellesis module.

Results: ECi-based clearing of hemi-mandible resulted in optimal transparency for microscope imaging, and preserved fluorophore signals labeled with click chemistry method. Multi-photon microscopy imaging allowed 3D visualization of fluorescent-labeled *P.g* and collagen fibers from PDL. Significantly more bacteria were detected by Zen Intellesis module in the infection group compared to the non-infection group.

Conclusion: This study presents a 3D imaging method that allows tracing of bacteria in murine model without sectioning. This method has the potential to be effectively utilized in different research fields of dentistry, such as in endodontics, oral pathology, or implantology.

Introduction

Periodontal disease is a prevalent chronic inflammatory disease that affects 42.2% of the adult population [1]. It is initiated by bacterial infection that in some cases causes a shift in the oral bacterial equilibrium, named dysbiosis, leading to pathological alveolar bone resorption [2]. Since the alveolar bone and the periodontal ligament (PDL) provide support to the tooth, bone resorption leads to reduction in tooth stability and eventually, tooth loss. Despite the wide consensus regarding the bacterial role in development of periodontitis and bone resorption, the exact mechanism and pathways by which bacteria cause bone resorption are not well understood. More specifically, it is currently unclear whether periodontal pathogens invade into the periodontal ligament (PDL) and thereafter to the bone or are generating uncontrolled inflammatory response by dysbiosis of the sulcular bacterial population.

The main reason for the lack of clarity of the bacterial role in PDL tissue degradation and bone resorption is mainly due to imaging challenges. The PDL is a soft tissue connecting the tooth and the bone. In order to understand the pathways of bacterial invasion, inflammation and the association to periodontitis, a method that enables 3D imaging of the bacteria inside the PDL is required. Current imaging methods include micro-CT, histology, and electron microscope [3-5]. Although micro-CT allows 3D imaging, it has limitations in obtaining information from mainly calcified tissue as well as in contrasting enhanced soft tissues and labeled objects. Selective bacterial staining can be performed on 2D tissue sections and requires harsh tissue processing and artefacts [6]; however, retrieving 3D information from 2D sections is challenging especially in a non-uniform tissue like the PDL. Finally, electron microscope methods enable some 3D information but are limited by their small region of interest and difficulty in imaging thick tissues [7].

The current study combined the use of various techniques to enable 3D imaging of bacteria inside the PDL without sectioning. Our first aim was to enable imaging through the bone. Tissue clearing methods, by decreasing a light scatter within a sample, allows optical sectioning of thick tissue to be possible [8]. In general, there are two main methods for achieving tissue clearing: aqueous-based and solvent-based clearing methods [8, 9]. The aqueous-based clearing method uses immersion of sample in an aqueous solution with a refractive index greater than 1.4 [8]. This approach works by removing lipids to achieve uniform light scattering within the tissue after matching of the refractive index with the solution [8, 9]. However, this method has a disadvantage of tissue shrinkage and suboptimal transparency of the tissue. Thus, in our study we utilized the second method, solvent-based clearing using ethyl-3-phenylprop-2-enoate (ethyl cinnamate, ECi). Studies have shown minimal hard tissue shrinkage, preservation of fluorescent signals and increased transparency [10, 11].

The two-photon microscopy has the advantage of deeper imaging depth and second-harmonic generation effect [12-14]. It can achieve tissue penetration depth of up to 2 mm because of less scattering of longer excitation wavelengths. It also minimizes photobleaching because the laser excites at a focal point [8]. Second-harmonic generation (SHG) effect occurs when two photons of the same wavelength energy excite non-linear material, which then generates a photon that is twice the energy of excitation photons [14, 15]. PDL consists mainly of Type I collagen,

which expresses high SHG signals due to its non-centrosymmetric structure [14, 16]. By collecting SHG signals from the collagen fibers, information regarding their orientation, size and distribution can be retrieved [16]. SHG signal collection through the cleared bone would therefore enable special analysis of the collagen network structure without any tissue staining or sectioning. Moreover, collecting both SHG and 2-photon emission from labeled structures enables colocalization and superimposition of different structures in 3D without distorting or compromising the sample.

Fluorescence labeling techniques have been widely used in microbiology studies to trace bacteria within a region of interest [17-19]. Due to its versatility, green fluorescent protein gene (GFP) has been most often used in fluorescent labeling but it has a limitation in that it requires oxygen for maturation of protein [20]. It cannot be used in periodontal microbiology studies because most periodontal pathogens are obligative anerobic bacteria that require handling in anerobic conditions. Geva-zatorsky et al. developed a fluorophore-labeling technique with click chemistry [21]. Click reaction refers to biocompatible, high-yielding, non-toxic spontaneous reaction [22]. Utilizing this reaction allows irreversible attachment of Click-IT fluorophore proteins (Invitrogen) onto anerobic bacterial cell surface constituents, which produces robust and stable fluorescent signals on anerobic cell surfaces [21, 23].

Porphyromonas gingivalis (*P. gingivalis*) is the most commonly used red complex bacteria for periodontal research due to its high virulence and presence in periodontal disease. They are gram-negative obligate anaerobes that express various virulent factors that can induce inflammation and tissue breakdown [24-26]. Previous studies have shown *P.gingivalis'* invasion into gingival epithelial tissues [27, 28], gingival fibroblasts [29], and pocket epithelial cells [30]. However, there are no studies showing its invasion into periodontal ligament space.

Therefore, in the present study, we developed a method to image and detect fluorescent-labeled *P. gingivalis* within the tooth-bone-PDL complex in 3D without any sectioning. Specifically, we focused on the most coronal region of PDL where non-uniform dense collagen network is exhibited, named dense collar [31, 32].

Materials and Methods

All animal experiments were performed in compliance with NIH's Guide for the Care and Use of Laboratory Animals and guidelines from the Harvard University Institutional Animal Care and Use Committee (Protocol no. 01840).

9-week-old male C57BL/6 mice were purchased from Charles River Laboratory (n=6). Mice were kept on a 12-hour light-dark cycle and were provided sterile food and distilled water ad libitum. The experiment had two experimental groups: one with an intact dense collar and the second with compromised dense collar. To compromise the PDL dense collar, mice were anesthetized with a mixture of ketamine and xylazine with intraperitoneal injection. Thereafter, a sterile 5-0 silk ligature was tied around the mandibular first molar (M1) at the cementoenamel junction (CEJ) level, keeping the knot mesiobuccally. After 24 hours, the 5-0 silk ligature was removed.

For both groups, 7-0 silk ligature was placed in an Eppendorf tube with fluorescently labeled bacteria (10^{10} CFU/mL) for 30 minutes. Ligature was then tied around M1 in the same manner as the 5-0 ligature. To increase the bacterial load, 5µl of 2% rich medium with 2% CMC (10^{10} CFU/mL of bacteria) was injected with a micropipette into the sulcus immediately after ligature placement.

For each experimental group, the intact and compromised, we had a control group with sterile 7-0 silk ligature. Mice were sacrificed by cervical dislocation 2 hours after the placement of the 7-0 ligature.

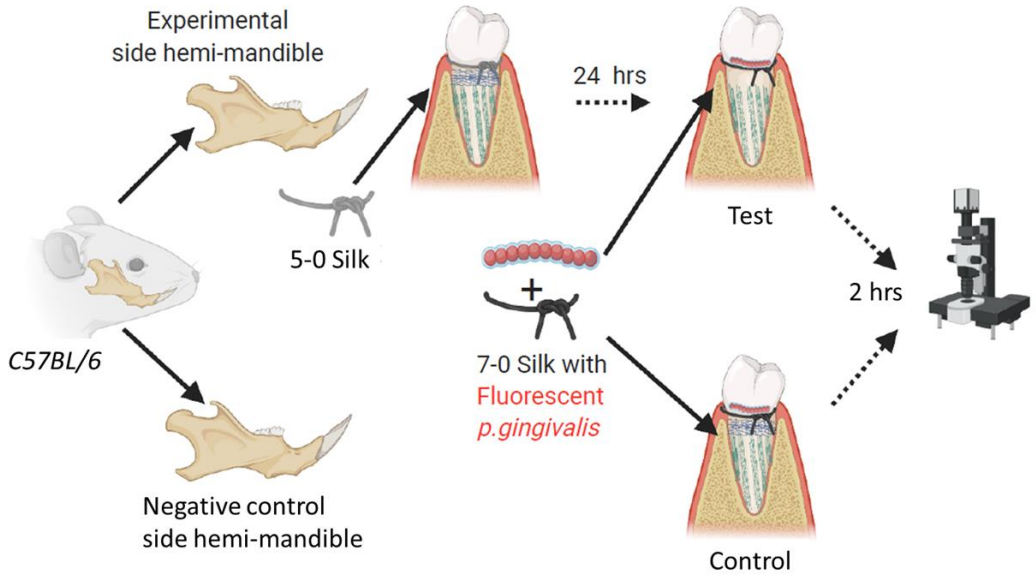

Figure 1. Experimental Design

Fluorescent labeling of *P.gingivalis* via Click chemistry

Fluorescently labeled *P. gingivalis* (strain w83, Kasper Lab stock) was prepared following a modified protocol established by Geva-Zatorsky et al. In brief, frozen *P. gingivalis* were struck onto brucella agar medium with 5% sheep blood (BMB) and were incubated for 4 to 7 days at 37 °C. One mL of pre-reduced rich medium containing sterile 7-0 silks and 100 µM N-azidoacetylgalactosamine-tetraacylated (GalNAz, Invitrogen C33365) were inoculated with colonies from BMB growth. After overnight incubation, bacteria were sedimented, washed 3 times with 1 mL phosphate buffered saline (PBS) containing 1% bovine serum albumin (BSA), then resuspended in 100 µL of PBS with 1 % BSA and 5 µM Click-IT™ Alexa Fluor™ 594 DIBO Alkyne (Invitrogen C10407), and incubated in the dark for 1 hour to allow for Click-IT™ reaction to occur. Cells were pelleted, washed twice with 1 mL PBS with 1% BSA, and once with 1 mL PBS. 7-0 silk with labeled bacteria (approximately 10^9 CFU) was suspended in 100 µl of rich medium with 2% carboxymethylcellulose (CMC) and kept in the dark in anaerobic conditions until placement around M1.

Optical tissue clearing with ECi-based clearing method [33]

Mandibles were dissected and split into two hemi-mandibles through the fibrous symphysis, and the surrounding tissue of each hemi-mandible was removed. The dissected hemi-mandibles

were fixed in 4% paraformaldehyde on a rocking table covered from light, at room temperature for 6 hours. After fixation, the specimens were dehydrated in a serial concentration of ethanol (50%, 70%, 100%, and 100% EtOH) for 16 hours each on a rocking table covered from light, at room temperature. Then, the specimens were immersed in a clearing agent, ethyl cinnamate (ethyl-3-phenylprop-2-enoate, Sigma-aldrich W243000-1KG-K), for a minimum of 12 hours until imaged with fluorescent microscope.

Multi-photon microscopy of cleared mandibles and image analysis

A custom-made hemi-mandible holder using a dental putty material (Exaflex Putty GC America 138305) was used to image every sample in a repeatable position. After the hemi-mandible was placed in the holder, it was immersed in ECi before imaging. ZEISS LSM 980 confocal microscope equipped with a Spectra-Physics Insight DeepSee X3 laser was used. For detection of Alexa Fluor™ 594 (bacteria), the laser was tuned to 850nm at 5.5% with pixel time of 0.51 µs. For SHG signal, the laser was tuned to 950nm at 8.0% with pixel time of 0.51 µs. To detect the emission signal, dual non-descanned GaAsP detectors preceded by 612-682 nm and 425-475 nm bandpass filters were used. The objective used was a Clr Plan-Neofluar 20x/1.0Corr immersion objective with correction collar set to RI = 1.56. All images were obtained in Z-stack to capture the 3D anatomy from the buccal bone into the root surface.

Bacteria detection by AI

ZEISS Zen Intellesis machine learning module was applied to detect bacteria signals in all images. It was trained to detect the fluorophore-labeled *P. gingivalis* in 2-photon data. First, the training was performed on multiple subsets of maximum intensity projection test images (with fluorescent bacteria) by repeatedly training the model to distinguish bacteria according to manual annotation of bacteria. Afterwards, training was repeated using the subsets of maximum intensity projection negative control data (without bacteria) to annotate the background.

Results

Mandibles were cleared using ECi. Since the clearance level could be adjusted by either changing the dehydration time or the dehydration agent, we tested different conditions to determine the optimal method for mandibular clearing. Optimal dehydration time was tested comparing 12-hour versus 16-hour dehydration sequences in each ethanol series. The 16-hour hemi-mandible was visually more transparent compared to the 12-hour hemi-mandible, which had more opaque hard tissue and vasculature (Figure 2D,E). When dehydration or immersion in ECi time was shortened, the hemi-mandible presented suboptimal optical transparency (Figure 2B). 1-propanol and ethanol were compared as dehydration agents. After 16 hours in 50%, 70%, 100%, and 100% of each agent, hemi-mandibles were immersed in ECi for 24 hours. Both groups' hemi-mandibles became optically transparent, and each hemi-mandible showed a gridline through its body of ramus (Figure 2C,E). Prolonging the dehydration time resulted in better clearing; however, this could impact the fluorescence signals. Based on our findings, 16 hours of ethanol dehydration resulted in adequate clearing and was short enough to preserve the fluorescence proteins.

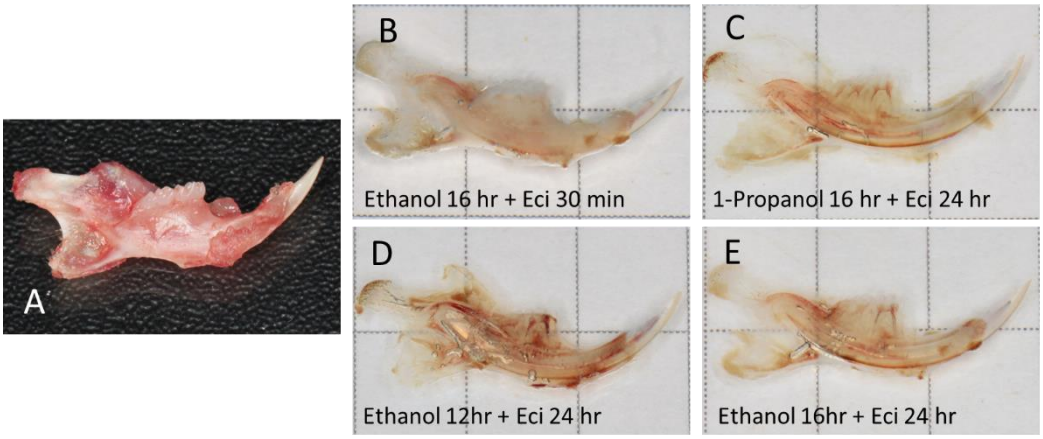

Figure 2. Eci-based clearing method comparison. (A) Immediately after dissection (B) 16 hours in series of ethanol gradient (50%, 70%, 100%, 100%), then 30 minutes in ethyl cinnamate. (C) 16 hours in series of 1-propanol gradient (50%, 70%, 100%, 100%), then 24 hours in ethyl cinnamate. (D) 12 hours in series of ethanol gradient, then 24 hours in ethyl cinnamate. (E) 16 hours in series of ethanol gradient, then 24 hours in ethyl cinnamate. Gridline = 0.5mm

To fluorescently label *P. gingivalis*, we used click chemistry technique based on GalNAz as a cell surface metabolite. Multiple fluorophore dyes were tested for click reaction. 1-photon microscopy images of Alexa Fluor™ 594 and Cy3 labeled *P. gingivalis* showed adequate signals, which confirmed formation of irreversible covalent bonds between GalNAz and fluorophores (Figure 3B,E). However, upon 2-photon microscopy and imaging inside the PDL, the fluorescence signal from Cy3 was difficult to detect compared to Alexa Fluor™ 594 (Figure 3F). This was due to the overlap between bacterial Cy3's emission wavelength and the auto-fluorescent signals emitted by collagens of soft tissue.

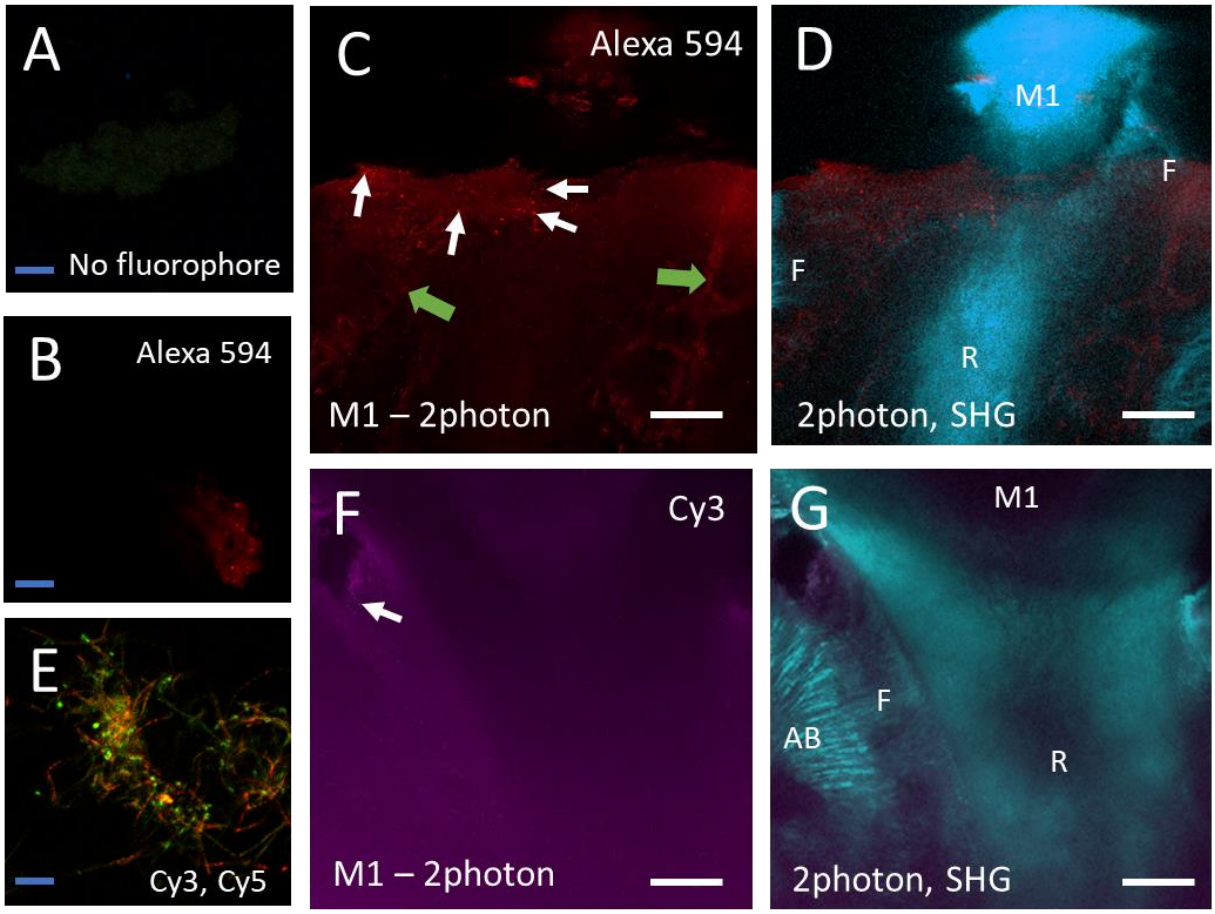

Figure 3. Fluorophore comparison. (A) *P. gingivalis* without fluorophore under 1-photon microscopy (B) *P. g* with Alexa fluor 594 (red) under 1-photon microscopy (C) *P.g* with Alexa fluor 594 within optically cleared M1 periodontium under 2-photon microscopy. Image was taken over the mesial root of M1. (D) SHG superimposed with (C). (E) *P.g* with Cy3 (green) and *F. nucleatum* with Cy5 (red) under 1-photon microscopy (F) *P.g* with Cy3 within optically cleared M1 under 2-photon microscopy. Image was taken over the distal root of M1. (G) SHG superimposed with (F).

Abbreviations: M1, first molar; AB, alveolar bone; R, root surface; F, collagen fibers; White arrow, bacterial signal; Green arrow, autofluorescence; Blue scale bar = 10 μm; White scale bar = 100 μm

The effect of ECi-clearing method on click-labeled bacteria was investigated. Fluorescent signals were detected from bacteria loaded onto silk threads before and after ECi-clearing (Figure 4C,D). Similar threads were used to inoculate bacteria into the PDL. No fluorophores were detected after clearing a sterile ligature (Figure 4B).

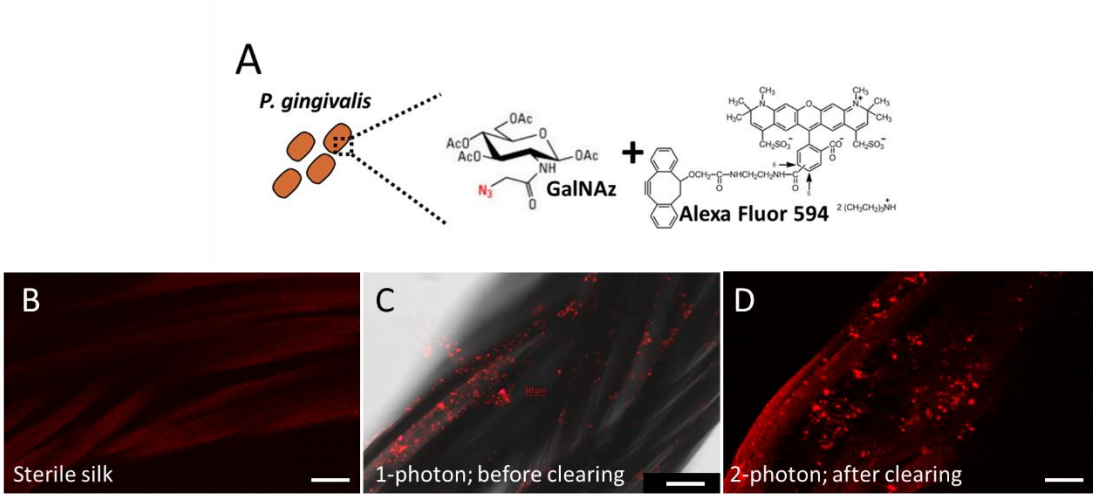

Figure 4. Alexa fluor 594 labeled *P. gingivalis* on a 7-0 silk ligature. (A) Illustration of *P.g* incorporating GalNAz as a metabolite on their CPS with click reaction. (B) Sterile silk ligature under the 2-photon microscopy. (C) Silk ligature with *P.g* before ECi-based clearing under 1-photon microscopy (D) Silk ligature with *P.g* after ECi-based clearing after 2-photon microscopy. Scale bar = 20 µm

To image the bacteria inside the PDL, multi-photon microscopy was used to capture 2-photon signals from bacteria and SHG signals from collagen fibers. The 2-photon signals were detected from the fluorescent-labeled *P.gingivalis* (Figure 5 grey arrow). Some auto-fluorescent signals were detected following the path of blood vessels (Figure 5 green arrow). The SHG signal from type I collagen fibers within the periodontal ligament and alveolar bone was detected (Figure 5C,F). Collagen fibers in the alveolar bone were mostly aligned horizontally (Figure 5 black arrow). In the crestal bone area, the collagen fibers from the alveolar bone extended and continued to the dense collar region, turning into the fibers of the dense collar (Figure 5 white arrow). These fibers were observed in the proximal 2D section, spanning the PDL space between tooth root and bone. PDL fibers apical of the dense collar were sparser and vertically oriented. For the intact dense collar (Figure 5C-E), most bacteria signals were found above the bone level, while the compromised dense collar group had a more apical distribution of bacteria signals found below the bone level (Figure 5E,H).

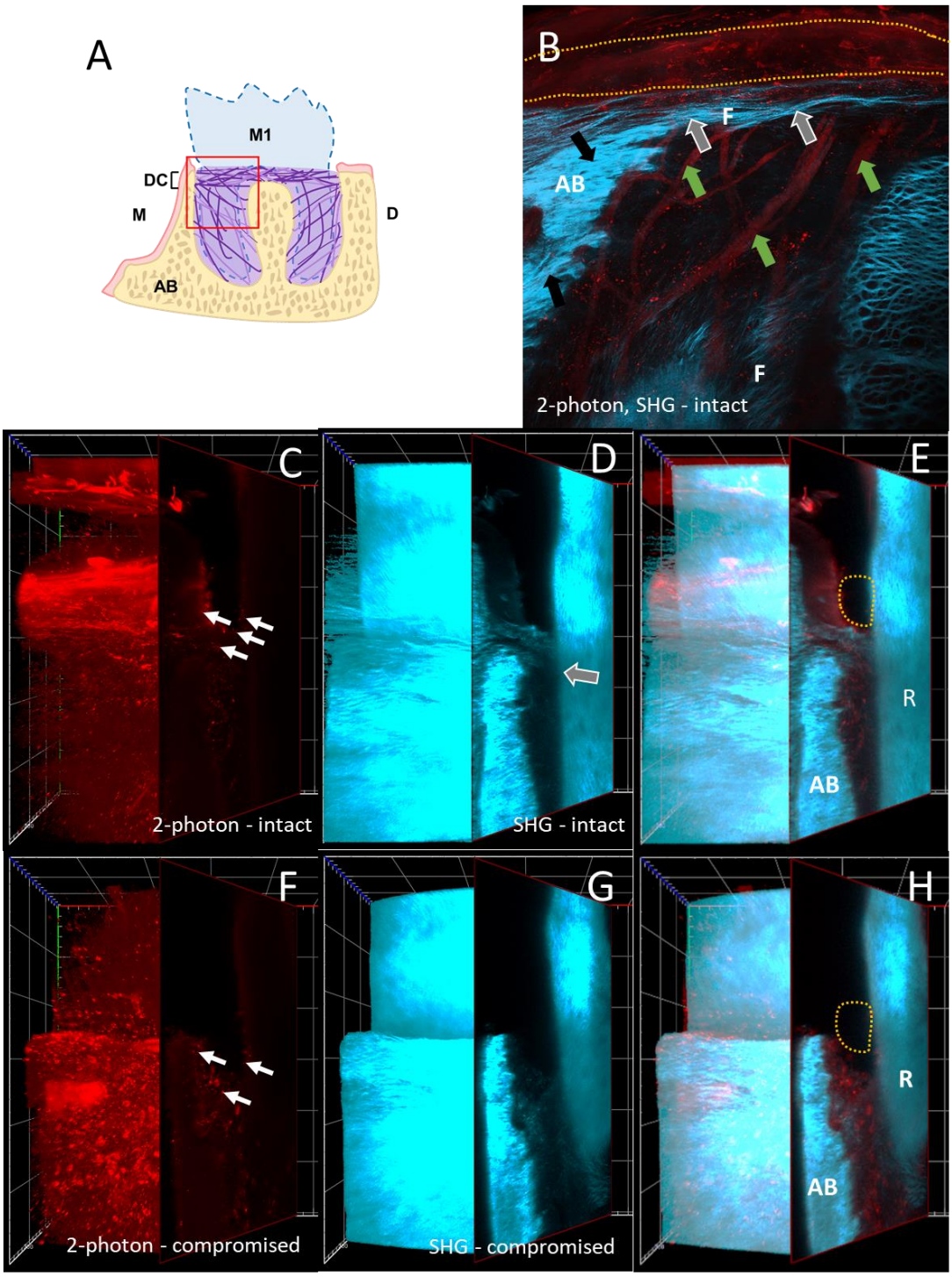

Figure 5. 2-photon (red) and Second Harmonic Generation (blue) signals in intact and compromised dense collar. (A) Red box depicts the location of microscopic images. (B) Superimposition of maximum intensity projection of 2-photon images and a single plane of SHG image. (C-E) Representative 3D images of ***intact*** dense collar. (F-H) Representative 3D images of ***compromised*** dense collar. (C,F) 2-photon signals from fluorescent-labeled bacteria, auto-fluorescence of blood vessels and other tissues are shown. (D,G) SHG image is showing the alveolar bone and collagen fibers. (E,H) Superimposition of 2-photon signals (C,F) and SHG image. (D,G)

Abbreviations: M1, first molar; DC, dense collar; M, mesial; D, distal; AB, alveolar bone; R, root surface; F, collagen fibers; Grey arrow, dense collar; Black arrow, fibers within AB; Green arrow, autofluorescence; White arrow, bacterial signal; Yellow dotted line, 7-0 silk ligature; Gridline: 100 μm

We used trained Zen AI Intellesis to identify bacterial signals within 2-photon images. First, the training was performed on the subset of test images (with labeled *P. gingivalis)* by manually annotating bacteria in the image so the AI could collect information about bacterial signals. Afterward, the AI was applied to the negative control data (without labeled *P. gingivalis*) to train background auto-fluorescence. The trained AI was considered validated when false positive detection of bacteria was less than 10 counts in each Z stack of negative control images. The representative images demonstrated that the trained AI detected multiple signals from the test group (Figure 6A), while it only detected one signal as bacteria from the negative control group (Figure 6B).

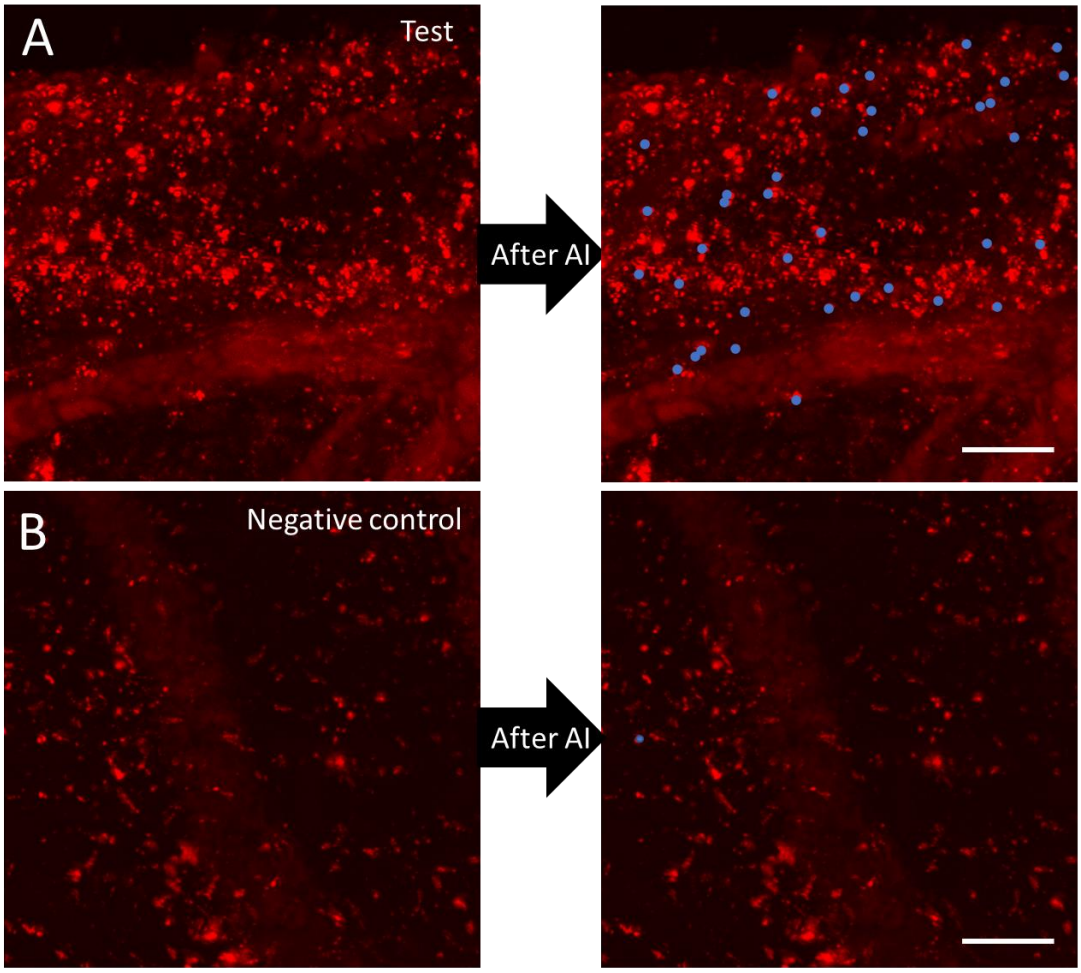

Figure 6. AI detection of bacteria from 2-photon microscopy images (A) Representative image of AI detecting bacteria signals from a subset of test image. (B) Negative control image shows auto-fluorescent signals with minimal detection from the AI. Blue dots, AI detected bacteria; Scale bar = 20 μm

The trained AI module was applied to all 2-photon Z-stack images obtained from each group. Bacteria signals identified by the AI were counted from all images and the mean was calculated from each group: compromised dense collar without *P.g*, intact dense collar without *P.g*, compromised dense collar with *P.g*, and intact dense collar with *P.g* (Figure 7). Both infection groups had significantly more bacteria count than the non-infection groups (unpaired t-test, $p<0.05$). The two infection groups and the two non-infection groups were not statistically significant from each other.

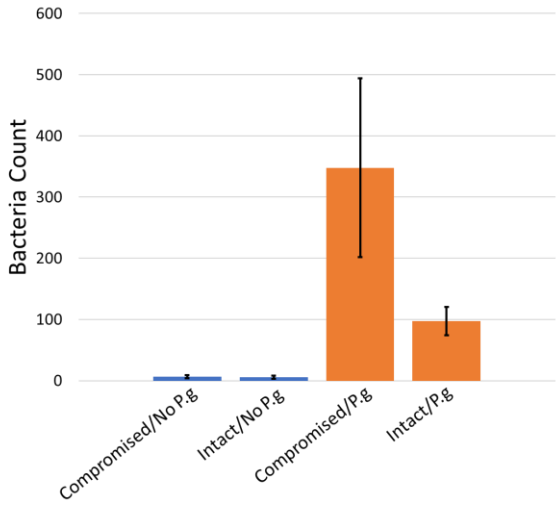

Figure 7. Bacteria detection comparison by ZEISS Zen AI module-Intellesis.

Discussion

This study presents a method to enable 3D imaging of bacteria inside the PDL without any sectioning and harsh tissue processing. This method, therefore, provides new pathways to study the association of structural tissue changes in the PDL and bone and their association with bacterial presence and inflammation, which is the core of periodontal disease. The presented ECi-based clearing method has two steps, dehydration and refractive index matching. There are different tissue dehydration methods: tetrahydrofuran (THF), methanol, 1-propanol or ethanol [8, 10, 34]. Since THF is toxic, and methanol is shown to decay fluorescent protein[10], we tested both 1-propanol and ethanol to achieve optimal clearing and adequate fluorophore preservation. Our results found minimal differences in clearing and fluorophore preservation between the two agents. 1-propanol's pH adjustment with triethylamine requires more cautious handling. Hence, we determined that ethanol was the less technique sensitive agent to clear the mandible.

Previous studies have demonstrated clearing of soft tissues, and long bones using an ECi-based clearing method [35]. However, there have been no attempts, to our knowledge, to clear mandibles with this method. The mandible is different from long bones since it encompasses two hard tissue and a soft tissue in one organ with different material penetration properties. Thus, to achieve optimal clearing of our sample, different clearing timelines were tested. Although soft tissue organs require 1-2 hours dehydration and ECi cycles [11], hard tissues are harder for liquids to penetrate uniformly, and therefore takes more hours to dehydrate. In this study, we compared

12-hour versus 16-hour cycles. When replicating this method, it is recommended that, depending on the researcher's sample size, dehydration hours be adjusted to achieve desired levels of optical transparency. We found 16-hour-cycle to be the most appropriate for a mouse model.

Click chemistry was used in order to label *P.gingivalis*. This specific method was developed to study host-commensal interactions within the anerobic intestine [21]. Unlike conventional fluorescent labeling, this method avoids use of oxygen to mature fluorescent proteins and can be executed under full anerobic conditions [21]. The click chemistry targets capsular polysaccharide (CPS) of anerobic bacteria to incorporate GalNAz as a metabolite, and uses biorthogonal click chemistry (BCC) to label fluorophore protein [21]. However, in Geva-Zatorsky et al., less than 50% of anaerobe species were reliably labeled, and *P. gingivalis* was not part of their tested species [21]. Hence, for our study, we tested and confirmed that *P.gingivalis* can successfully be labeled. Recently, the Kasper Lab developed click reactions that can tag fluorophores onto various bacterial cell surface constituents: peptidoglycan (PGN) and lipopolysaccharide (LPS) [23]. Utilizing this technique can potentially benefit periodontal studies by allowing multiple periodontal pathogens to be labeled and tracked simultaneously.

To optimize imaging of the bacteria within the PDL, we tested different fluorophore proteins. The PDL consists of blood vessels, collagen fibers, and other extracellular matrix (ECM) [36], which emit strong auto-fluorescent signals. According to Richardson and Lichtman, autofluorescence comes from various biomolecules, such as NADPH, collagen, or tyrosine [8]. We therefore needed to find a fluorophore that could be distinguishable enough from the strong background signals. We labeled bacteria with Cy3, Cy5 and Alexa Fluor™ 594, and compared their emission signals. 1-photon confocal microscopy was used to confirm successful click reaction, and 2-photon microscopy to image *in-situ* (Figure 3B,C,E,F). Signals from Cy3 and Cy5 fluorophores were indistinguishable from the background autofluorescence (Figure 3F). Alexa Fluor™ 594, on the other hand, had better distinguishable emission of bacteria (Figure 3C). However, autofluorescence still remained as a limitation especially from single cells like red blood cells, osteocytes, and potentially osteoblasts, osteoclast, and fibroblasts [37]. We needed to find an approach that would enable us to distinguish the bacteria from other auto-fluorescent cells. Since bacteria are mostly smaller than the rest of the auto-fluorescent cells and emit signals in a higher intensity, we utilized machine learning based segmentation protocol to distinguish the bacteria from the other cells. Zeiss Zen Intellesis is a versatile machine learning module that is utilized to successfully segment various anatomical structures, such as vessels in murine brain [38] or cardiomyocytes in porcine heart [39]. Thus, we used this module to detect *P. gingivalis*. Integrating this morphological and image analysis tool while removing user's bias is a powerful method, especially with challenging data sets as in our case. Our approach was to train the algorithm to identify bacteria based on pixel intensity, shape, texture, and edge contrast [38]. This way, we could increase the certainty that the selected dots were, in fact, labeled bacteria (Figure 6A).

This study's ligature model successfully depicted the dense collar with SHG imaging to differentiate intact versus compromised dense collars without signs of bone loss (Figure 5D,G). The 24-hour duration of 5-0 silk ligature was appropriate to solely compromise the dense collar.

Selective removal of dense collar was significant in that it allowed further study to be possible. Although we have a lack of sample size, our preliminary data shows that there was a trend of more bacteria being detected in the compromised dense collar group compared to the intact group (Figure 7). We plan future studies to delve into deeper analysis of the pattern and amount of bacteria distribution within the network of periodontal ligament.

Conclusion

In the present study, we demonstrated a successful 3D imaging protocol by combination of ECi-based clearing method, click chemistry to fluorescently label and finally, Zen Intellesis module to detect bacteria. We anticipate that our study design will allow to investigate the role of dense collar in periodontal disease. Replicating this study with a bigger sample size may provide new knowledge in regard to the role of dense collar in regulating bacterial invasion. Moreover, modification of this method could expand its use in dental research, such as in endodontics, oral pathology, or in studies of peri-implant disease.

References

1. Eke, P.I., et al., *Periodontitis in US Adults: National Health and Nutrition Examination Survey 2009-2014.* The Journal of the American Dental Association, 2018. **149**(7): p. 576-588.e6.
2. Tonetti, M.S., H. Greenwell, and K.S. Kornman, *Staging and grading of periodontitis: Framework and proposal of a new classification and case definition.* Journal of clinical periodontology, 2018. **45**: p. S149-S161.
3. Noiri, Y., et al., *Localization of Porphyromonas gingivalis-carrying fimbriae in situ in human periodontal pockets.* Journal of dental research, 2004. **83**(12): p. 941-945.
4. Zhu, C., et al., *The therapeutic role of baicalein in combating experimental periodontitis with diabetes via Nrf2 antioxidant signaling pathway.* Journal of periodontal research, 2020. **55**(3): p. 381-391.
5. Hiyari, S., et al., *Heritability of periodontal bone loss in mice.* Journal of periodontal research, 2015. **50**(6): p. 730-736.
6. Noiri, Y., et al., *An immunohistochemical study on the localization of Porphyromonas gingivalis, Campylobacter rectus and Actinomyces viscosus in human periodontal pockets.* Journal of Periodontal Research, 1997. **32**(7): p. 598-607.
7. Noiri, Y. and S. Ebisu, *Identification of periodontal disease-associated bacteria in the "plaque-free zone".* Journal of periodontology, 2000. **71**(8): p. 1319-1326.
8. Richardson, D.S. and J.W. Lichtman, *Clarifying Tissue Clearing.* Cell, 2015. **162**(2): p. 246-257.
9. Costantini, I., et al., *In-vivo and ex-vivo optical clearing methods for biological tissues: review.* Biomed Opt Express, 2019. **10**(10): p. 5251-5267.
10. Masselink, W., et al., *Broad applicability of a streamlined ethyl cinnamate-based clearing procedure.* Development, 2019. **146**(3).
11. Klingberg, A., et al., *Fully automated evaluation of total glomerular number and capillary tuft size in nephritic kidneys using lightsheet microscopy.* Journal of the American Society of Nephrology, 2017. **28**(2): p. 452-459.
12. So, P.T., et al., *Two-photon excitation fluorescence microscopy.* Annual review of biomedical engineering, 2000. **2**(1): p. 399-429.
13. Steven, P., et al., *Imaging corneal crosslinking by autofluorescence 2-photon microscopy, second harmonic generation, and fluorescence lifetime measurements.* Journal of Cataract & Refractive Surgery, 2010. **36**(12): p. 2150-2159.
14. Zoumi, A., A. Yeh, and B.J. Tromberg, *Imaging cells and extracellular matrix in vivo by using second-harmonic generation and two-photon excited fluorescence.* Proc Natl Acad Sci U S A, 2002. **99**(17): p. 11014-9.
15. Campagnola, P.J. and L.M. Loew, *Second-harmonic imaging microscopy for visualizing biomolecular arrays in cells, tissues and organisms.* Nat Biotechnol, 2003. **21**(11): p. 1356-60.
16. Dudenkova, V.V., et al., *Examination of Collagen Structure and State by the Second Harmonic Generation Microscopy.* Biochemistry (Mosc), 2019. **84**(Suppl 1): p. S89-s107.
17. Yilmaz, Ö., et al., *Intercellular spreading of Porphyromonas gingivalis infection in primary gingival epithelial cells.* Infection and immunity, 2006. **74**(1): p. 703-710.
18. Yao, á., et al., *Porphyromonas gingivalis infection sequesters pro-apoptotic Bad through Akt in primary gingival epithelial cells.* Molecular oral microbiology, 2010. **25**(2): p. 89-101.

19. Ilievski, V., et al., *Identification of a periodontal pathogen and bihormonal cells in pancreatic islets of humans and a mouse model of periodontitis.* Sci Rep, 2020. **10**(1): p. 9976.
20. Tsien, R.Y., *The green fluorescent protein.* Annual review of biochemistry, 1998. **67**(1): p. 509-544.
21. Geva-Zatorsky, N., et al., *In vivo imaging and tracking of host-microbiota interactions via metabolic labeling of gut anaerobic bacteria.* Nat Med, 2015. **21**(9): p. 1091-100.
22. Takayama, Y., K. Kusamori, and M. Nishikawa, *Click Chemistry as a Tool for Cell Engineering and Drug Delivery.* Molecules (Basel, Switzerland), 2019. **24**(1): p. 172.
23. Hudak, J.E., et al., *Illuminating vital surface molecules of symbionts in health and disease.* Nature microbiology, 2017. **2**(9): p. 17099.
24. Hajishengallis, G. and R.J. Lamont, *Beyond the red complex and into more complexity: the polymicrobial synergy and dysbiosis (PSD) model of periodontal disease etiology.* Molecular oral microbiology, 2012. **27**(6): p. 409-419.
25. Séguier, S., et al., *Is collagen breakdown during periodontitis linked to inflammatory cells and expression of matrix metalloproteinases and tissue inhibitors of metalloproteinases in human gingival tissue?* Journal of periodontology, 2001. **72**(10): p. 1398-1406.
26. Polak, D., et al., *Mouse model of experimental periodontitis induced by Porphyromonas gingivalis/Fusobacterium nucleatum infection: bone loss and host response.* Journal of clinical periodontology, 2009. **36**(5): p. 406-410.
27. Belton, C.M., et al., *Fluorescence image analysis of the association between Porphyromonas gingivalis and gingival epithelial cells.* Cellular microbiology, 1999. **1**(3): p. 215-223.
28. Lamont, R.J., et al., *Porphyromonas gingivalis invasion of gingival epithelial cells.* Infect Immun, 1995. **63**.
29. Amornchat, C., et al., *Invasion of Porphyromonas gingivalis into human gingival fibroblasts in vitro.* Journal of the International academy of periodontology, 2003. **5**(4): p. 98-105.
30. Sandros, J., et al., *Porphyromonas gingivalis invades human pocket epithelium in vitro.* J Periodontal Res, 1994. **29**.
31. Naveh, G.R.S., et al., *Nonuniformity in ligaments is a structural strategy for optimizing functionality.* Proc Natl Acad Sci U S A, 2018. **115**(36): p. 9008-9013.
32. Connizzo, B.K. and G.R.S. Naveh, *In situ AFM-based nanoscale rheology reveals regional non-uniformity in viscoporoelastic mechanical behavior of the murine periodontal ligament.* J Biomech, 2020. **111**: p. 109996.
33. Au - Xu, H., et al., *3D Imaging of PDL Collagen Fibers during Orthodontic Tooth Movement in Mandibular Murine Model.* JoVE: p. e62149.
34. Ertürk, A., et al., *Three-dimensional imaging of solvent-cleared organs using 3DISCO.* Nat Protoc, 2012. **7**(11): p. 1983-95.
35. Hofmann, J., et al., *Efficient Tissue Clearing and Multi-Organ Volumetric Imaging Enable Quantitative Visualization of Sparse Immune Cell Populations During Inflammation.* Frontiers in immunology, 2021. **11**: p. 3564.
36. Newman, M.T., H.; Klokkevold, P.; Carranza, F., *Carranza's Clinical Periodontology 12th Edition*. 2015: Elsevier.
37. Lang, N.P. and J. Lindhe, *Clinical Periodontology and Implant Dentistry* 6th Edition ed. 2015: Wiley Blackwell.

38. Henriksen, B.L., K.H. Jensen, and R.W. Berg, *Vasculature-staining with lipophilic dyes in tissue-cleared brains assessed by deep learning.* 2020.
39. Citerni, C., et al., *Characterization of Atrial and Ventricular Structural Remodeling in a Porcine Model of Atrial Fibrillation Induced by Atrial Tachypacing.* Frontiers in Veterinary Science, 2020. **7**(179).